Towards personalized drug delivery via semi-solid extrusion: Exploring poly(vinyl alcohol-co-vinyl acetate) copolymers for

European Journal of Pharmaceutical Sciences 192 (2024) 106645

Contents lists available at ScienceDirect

European Journal of Pharmaceutical Sciences

journal homepage: www.elsevier.com/locate/ejps

Towards personalized drug delivery via semi-solid extrusion: Exploring poly(vinyl alcohol-co-vinyl acetate) copolymers for hydrochlorothiazide-loaded films

Karin Korelc [a,1,*], Bjarke Strøm Larsen [a,1], Anna-Lena Heintze [a,b], Åke Henrik-Klemens [c,d], Jakob Karlsson [d], Anette Larsson [c,d], Ingunn Tho [a]

[a] Department of Pharmacy, University of Oslo, P.O. Box 1068 Blindern, Oslo 0316, Norway
[b] Department of Pharmacy, Julius-Maximilians-University of Würzburg, Germany
[c] FibRe Centre for Lignocellulose-Based Thermoplastics, Department of Chemistry and Chemical Engineering, Chalmers University of Technology, Sweden
[d] Department of Chemistry and Chemical Engineering, Chalmers University of Technology, Sweden

ARTICLE INFO

Keywords:
Block copolymers
Modified drug release
Mechanical properties
HT29-MTX cell line
Permeability
Biocompatibility

ABSTRACT

The increasing need for personalized drug delivery requires developing systems with tailorable properties. The copolymer poly(vinyl alcohol-co-vinyl acetate) (PVA/PVAc) allows for adjusting the monomer ratio. This study explored the effect of vinyl alcohol (VA) and vinyl acetate (VAc) monomer ratio on the properties of hydrochlorothiazide (HCT) films. Five copolymers with different VA/VAc ratios were selected and characterized. Semi-solid extrusion was employed as a method for the preparation of HCT-PVA/PVAc films to address the challenges of HCT's low water solubility, high melting point, and low permeability. All copolymers were suitable for semi-solid extrusion, however, the mechanical properties of films with higher VA proportions were more suitable. The drug was found to be homogeneously distributed on a micrometer level throughout the prepared films. It was found that using different monomer ratios in the copolymer allows for drug release tuning – higher VA proportions showed an increased rate of drug release. Experiments through HT29-MTX cell monolayers revealed differences in HCT permeability between the different formulations. In addition, no cytotoxicity was observed for the tested formulations. The results highlight the effect of monomer ratio on film properties, providing valuable guidance for formulators in selecting PVA/PVAc copolymers for achieving desired high-quality films. In addition, varying the monomer ratio allows tuning of the film properties, and can be applied for personalization, with flexible-dose adjustment and design of appealing shapes of the pharmaceutics, not least attractive for pediatric drug delivery.

1. Introduction

The increasing need for individualized dosage forms calls for tailoring materials and techniques to ensure adequate final properties of drug formulations and properly controlled drug delivery systems (DDS). Polymers are one of the most commonly used materials in the three-dimensional printing (3DP) of solid dosage forms, e.g. films (Pitzanti et al., 2022). The selection of polymers affects the final characteristics of a product, for example, release pattern and mechanical properties. The ideal polymer for 3D printing should possess essential traits such as biocompatibility, compatibility with the active pharmaceutical ingredient (API), precise control over drug release, and excellent printability (Pitzanti et al., 2022).

Among the pharmaceutically interesting polymers for controlled DDSs is poly(vinyl alcohol-co-vinyl acetate) (PVA/PVAc), a copolymer formed of two different types of monomers, vinyl alcohol (VA) (see Fig. 1a) and vinyl acetate (VAc) (see Fig. 1b), linked together to the same polymer chain. PVA/PVAc is obtained by polymerization of VAc to PVAc and subsequent partial hydrolysis of VAc to VA (Mansur et al., 2008). PVA is an attractive, highly polar polymer in pharmaceutical applications with good chemical resistance, excellent film-forming properties, water-solubility, biocompatibility, and biodegradability (Cano et al.,

* Corresponding author.
E-mail address: karin.korelc@farmasi.uio.no (K. Korelc).
[1] Co-first author (equal contribution to this work).

https://doi.org/10.1016/j.ejps.2023.106645
Received 14 August 2023; Received in revised form 2 November 2023; Accepted 5 November 2023
Available online 18 November 2023

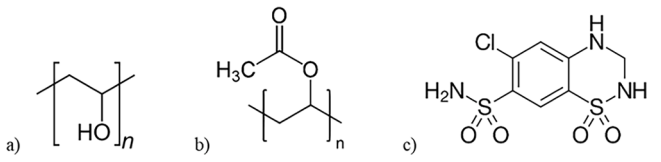

Fig. 1. Structures of (a) poly(vinyl alcohol, (b) poly(vinyl acetate), and (c) hydrochlorothiazide.

2015; Fernandes et al., 2022). Due to its suitable melting point, it has a wide interest in 3DP, especially in fused-deposition modeling (Pitzanti et al., 2022). PVAc has similarly good film-making properties and biodegradability to a certain extent, but is a non-polar polymer (Squillace et al., 2020).

The hydrolysis degree, i.e. the fraction of VA repeating units, allows for modification of chemical properties and water solubility, depending on the proportion of each monomer (Mansur et al., 2008). Generally, the aqueous solubility of the polymer increases as the proportion of VA increases. However, with high VA proportions (e.g. 98 % VA), the crystalline proportion in the polymer increases, increasing inter- and intra-molecular hydrogen bonding and decreasing polymer solubility. To dissolve copolymers with approximately 98 % VA in water, higher temperatures (e.g. 80 °C) are required (Briscoe et al., 2000). It is described that the intermolecular interactions are re-formed with subsequent cooling and time, which is recognized as an increase in the apparent viscosity over time. The behavior of the copolymers varies additionally on their average molecular weight (Mw), polydispersity index, average VAc and VA sequence lengths (i.e. directly related to the distribution of the monomer units in the copolymer chains), polymerization degree, and other characteristics (Atanase et al., 2015).

Semi-solid extrusion (SSE) is a 3DP technique allowing for the small-scale production of dosage forms to meet individual patients' needs (Sjöholm et al., 2022). In SSE, a gel or paste with suitable rheological properties is extruded through the die (usually at room temperature) and shaped into a desired form, typically designed with computer-aided design (CAD) software (Gkaragkounis and Fatouros, 2023). The printed paste is left to solidify, gaining physical strength and final form as liquid components evaporate. An additional step is required in SSE compared to other types of 3DP (such as fused-deposition modeling), i.e., dispersing or dissolving all the components, before feeding the paste into the drop generator. The key considerations to optimize the printing process are travel speed, nozzle diameter, and extrusion rate. SSE offers a large variety of 3D structures like tablets, chewable formulations, orodispersible films, suppositories etc. (Gkaragkounis and Fatouros, 2023; Govender et al., 2021). Compared to the commonly used melt-based extrusion 3D printing, this technique offers a distinct advantage: it operates at a lower processing temperature, making it suitable for thermolabile compounds. SSE enables personalization of pharmaceutics for specific patients or patient groups, as the SSE allows adopting the size, shape, and formulation properties such as drug release rate, texture, and drug loading to a larger extent compared to many other printing technologies (El Aita et al., 2020; Gkaragkounis and Fatouros, 2023; Johannesson et al., 2021). Moreover, compared to well-established solvent-casting methods for film preparation, SSE demonstrates superior mass uniformity and enhanced flexibility, particularly concerning patient-centricity. SSE has recently gained significant attention in pediatric drug delivery due to its versatile applications, such as its unique possibility to prepare chewables, which pediatric patients have shown to prefer (Rahman and Quodbach, 2021).

Hydrochlorothiazide (HCT; Fig. 1c) is a diuretic drug used to treat hypertension and heart failure, kidney, and liver diseases. HCT is featured on the "WHO Model List of Essential Medicines for Children ("WHO Model List of Essential Medicines for Children," 2021), making it a valuable target for the development of new drug delivery systems that would be relevant for personalization and improvement of the current therapy with HCT. It belongs to the class IV of the Biopharmaceutical Classification System (BCS) (Teixeira et al., 2020), posing both solubility and permeability issues when developing formulations. Additionally, it is light-sensitive and is subjected to degradation in the aqueous media within the pH range of 4–10 (Gumieniczek et al., 2018). HCT is also unsuitable for pharmaceutical techniques requiring elevated temperature, such as hot-melt extrusion, as it decomposes at higher temperatures, i.e. 314 °C (Macedo et al., 2001).

It is well-known that the ratio of vinyl alcohol to vinyl acetate repeating units in PVA/PVAc and its monomer distribution significantly impact the physiochemical properties of the copolymer. However, the influence of the degree of hydrolysis (DH) on drug formulations, specifically SSE printed films, remains unexplored. This study aimed to investigate the properties of SSE printed films, containing HCT as a model drug and utilizing five different PVA/PVAc copolymers with PVA/PVAc ratios ranging from 35/65 to 98/2. By employing SSE, the films were prepared without subjecting HCT to excessive heating, enabling the exploration of personalized drug delivery possibilities. The copolymers were characterized to allow linking the physicochemical and biopharmaceutical characteristics of the film formulations to the polymer characteristics. Biocompatibility and permeability were evaluated using the HT29-MTX cell line.

2. Materials and methods

2.1. Materials

PVA/PVAc copolymers with five different monomer ratios (Table 1) were obtained from Kuraray Poval™ (Frankfurt, DE). HCT and phosphate-buffered saline (PBS) tablets were obtained from Sigma Aldrich (St. Louis, MO, USA). Sodium chloride and acetonitrile were obtained from VWR International (Darmstadt, Germany). DMSO-d6 (99.9 % D atoms) and green food color were purchased from Merck (Darmstadt, Germany) and Dr. Oetker (Bielefeld, DE), respectively.

For the cell experiments, Hanks' balanced salt solution (HBSS), Trypsin-EDTA salt solution, inactivated fetal bovine serum (FBS), penicillin-streptomycin (10,000 U/mL), non-essential amino acid (100x) (NEAA) and DMSO were obtained from Merck (Darmstadt, DE). Thiazolyl Blue Tetrazolium Bromide (MTT reagent) and 5-(6)-carboxyfluorescein (CF) were obtained from Sigma Aldrich (St. Louis, MO, USA). Dulbecco's Modified Eagle Media (DMEM) with GlutaMAX™ supplement and trypan blue were obtained from Thermo Fisher Scientific. HT29-MTX cell line was kindly provided by Dr. Thécla Lesuffleur (INSERM UMR S 938, FR).

Table 1
Overview of the poly(vinyl alcohol-co-vinyl acetate) samples received from the supplier.

Product name	Declared DH (%)	Abbreviation used	Viscosity (mPa × s)*
Kuraray Poval™ LM-25	35	PVA35	3.0–4.0
Kuraray Poval™ LM-22	50	PVA50	3.0–4.0
Kuraray Poval™ 5–74	74	PVA74	4.2–5.0
Kuraray Poval™ 4–88	88	PVA88	3.5–4.5
Kuraray Poval™ 4–98	98	PVA98	4.0–5.0

* viscosity of the 4 % solution at 20 °C, provided by the supplier (Kuraray Poval, 2023).

2.2. Methods

2.2.1. Polymer characterization

2.2.1.1. Attenuated total reflectance-Fourier Transform Infrared Spectroscopy (ATR-FTIR). The copolymers (powder) were analysed using ATR-FTIR (Nicolet iS5, ThermoFisher Scientific, MA, USA). The spectra were recorded in the transmittance mode with a resolution of 4 cm^{-1} and 16 scans in the wavenumber interval between 500 and 4000 cm^{-1}.

2.2.1.2. ^{1}H NMR. 10 mg of polymer was dissolved in 0.5 ml of DMSO-d6. The solutions were transferred to 5 mm tubes and the NMR spectra were recorded on a Bruker Avance NEO spectrometer 600 MHz at 25 °C. A pulse width of 30 ° was used, and acquisition and relaxation times were 3 s and 3 s, respectively. Baseline correction was done with a linear function, and the central solvent peak of DMSO at 2.5 ppm was used for chemical shift calibration. The degree of hydrolysis was calculated according to the literature (van der Velden and Beulen, 1982) (see Eq. (1)), where acetate and methylene protons were integrated according to Fig. S1 (Supplementary material).

$$Degree\ of\ hydrolysis\ (\%) = 100\% - \frac{acetate\ protons}{3} \div \frac{methylene\ protons}{2} \quad (1)$$

The sequence distribution of (OH) and (OAc) was quantified by integrating the methylene peaks corresponding to three different dyads and their mole fractions ((OH,OH), (OH,OAc) and (OAc,OAc), see Supplementary material, Fig. S1) Moritani and Fujiwara, 1977; van der Velden and Beulen, 1982). The number average sequence lengths for the alcohols and acetates were calculated according to Eqs. (2)–((4), where (OH) and (OAc) represent the mole fractions of vinyl alcohol and vinyl acetate, respectively. n_{OH} and n_{Ac} are the number-average alcohol and acetate sequence lengths, respectively. As the methylene dyad of (OH, OAc) is less separated in the ^{1}H compared to ^{13}C NMR (Van der Velden and Beulen, 1982), their quantification should be seen as semi-quantitative in this study.

$$(OH) = (OH, OH) + \frac{(OH,\ OAc)}{2} \quad (2)$$

$$n_{OH} = \frac{2(OH)}{(OH, OAc)} \quad (3)$$

$$n_{OAc} = \frac{2(OAc)}{(OH, OAc)} \quad (4)$$

2.2.1.3. Size exclusion chromatography (SEC). The SEC was employed to determine the molecular mass (Mw) of copolymers. An aqueous solvent with 10 mM NaCl and 0.002 % NaN_3 was used as a mobile phase. Samples were prepared in the respective mobile phase and left to stir overnight to solubilize the polymer. The mobile phase was filtered and degassed before the analysis. Two inline filters were used, one Millipore VM 0.05 μm filter and one Sartorius CA 0.45 μm before the column. The samples were filtered through a syringe filter (Acrodisc 13 mm minispike with 0.45 μm wwPTFE) before being injected in a TSKgel GMPPWXL 7.8 × 300 mm column with a particle size of 13 μm. The flow rate used was 0.5 ml/min and the total injection volume was 100 μl. Three detectors were used for the analysis: a DAWN HELEOS-II multi-angle laser light scattering detector, a Viscostar 3 viscometer and an Optilab T-rEX refractive index detector. The data was analysed using the software ASTRA (version 5.3.4.).

2.2.1.4. Dynamic light scattering. Dynamic light scattering was performed with ZetaSizer Nano Series (Malvern Instruments Ltd., Malvern, UK) to determine the potential formation of nanostructures of co-polymers in water and the hydrodynamic diameter of such structures. 1 % w/V polymer dispersions were prepared in milliQ water. The measurements were performed at a 173 ° backscatter angle at 25 °C with three subsequent runs for each sample, and an average of three values were noted for each sample. The experiments were run in triplicates. The mean and standard deviation (SD) were calculated for each sample.

2.2.2. Selection of a solvent to simultaneously dissolve HCT and PVA/PVAc

Preliminary studies were performed to find a common solvent for HCT and the five copolymers. Water was used as the initial solvent, however, due to the poor water solubility of HCT, other solvents like ethanol, 50 % ethanol/water, methanol, acetone, tert-butanol/ethanol 10:1 and 5:1 were also investigated. The best choice of these solvents was determined empirically by evaluating the appearance of the solutions and was later used to prepare the film formulations.

2.2.3. Preparation of films

The wet film formulations were prepared by using 40 % m/V copolymer PVA/PVAc, 5 mg/mL HCT in 50 % v/v ethanol/water, with one droplet of the green food color per 10 mL solution. The five film formulations are referred to as PVA35, PVA50, PVA74, PVA88 and PVA98, where the number corresponds to the DH, i.e., the hydrolysed mol % of PVAc, which is equal to the mol % ratio of PVA in the copolymer (see Table 1). Due to difficulties dissolving an adequate amount of PVA98 in this solvent, the polymer and drug concentrations in this formulation were reduced by half (20 % w/v and 2.5 mg/mL, respectively). However, the polymer-to-drug ratio was maintained consistent with the other formulations.

The film formulations were prepared in the following way: 8 g of the polymer was weighed and added to 10 mL of water under magnetic stirring (4 g in the case of PVA98). The PVA88 and PVA98 samples needed to be heated to achieve solubilization for 2 h at 80 °C and 120 °C, respectively, and evaporated water was replaced. A solution of HCT (10 mg/mL – 5 mg/mL for PVA98 formulation) in ethanol (10 mL) was added to the PVA/PVAc samples, and the resulting drug-polymer mixture was left overnight under magnetic stirring. The PVA88 and PVA98 samples were re-heated for 1 h at the same conditions as before to achieve complete dispersion of both components in the solvent. Finally, two drops of green color were added to enhance the visual properties of the semi-solid extruded films in the shamrock shape, and the solution was stirred until having reached a homogeneous and clear appearance.

2.2.4. Viscosity of polymeric dispersions and wet film formulations

The dynamic viscosity of the aqueous polymer dispersions (10 % w/V) in water and the wet film formulations (40 % w/V polymer with 5 mg/mL HCT in 1:1 water:ethanol) was measured using a Brookfield viscometer DV2T (Middleboro, MA, USA) with the spindle CPA-52Z at 25 °C. 2 min single-point measurements were performed by using 500 μL of the wet film formulations and polymer dispersions in water at applying 2 rpm and 100 rpm, respectively, to achieve a suitable torque in respect to the concentrations used. The polymer dispersions obtained from PVA35 and PVA50 were measured at 200 rpm due to too low viscosity for measurement at the speed of 100 rpm.

2.2.5. 3D printing of films and storage

The films were SSE 3D printed using SSE ZMorph 2 (ZMorph, Wroclaw, PL) in the shape of a shamrock with four clovers, designed using Autodesk Fusion 360 (Autodesk, San Rafael, California, USA) (see Fig. 2), and transferred to Voxelizer 2 (ZMorph, Wroclaw, PL) to finalize the printing parameters. The gel consistency was set to 100 % with one layer count, a layer height of 1 mm, and a path width of 0.8 mm. The travel and print speeds were set to 50 mm/s and 1.0 mm/s, respectively. The films were printed onto the printing surface (smooth side of Bench Surface Protector, VWR International, FR), and were allowed to dry at ambient conditions for 24 h. One clover of a shamrock was considered a

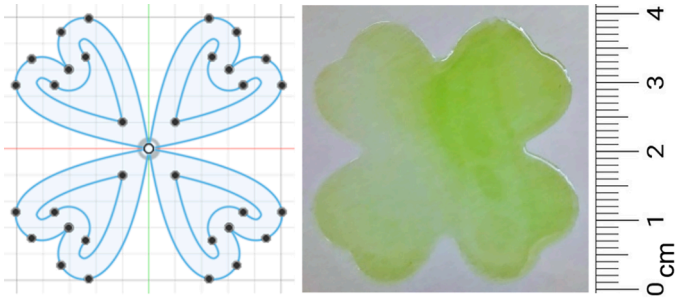

Fig. 2. The sketch of the shamrock in the Fusion 360 and an example of a semi-solid extruded dried film on a printing surface. A scale bar is added to the figure.

single dose, with the theoretical content of HCT of 1.2 mg (0.6 mg for PVA98).

The printed and dried films were stored in a plastic box protected from light at the room temperature (RT) and approx. 33 % relative humidity (overly saturated $MgCl_2$ * 6 H_2O solution).

2.2.6. Characterization of the films

2.2.6.5. Mass and thickness. Films ($n \geq 8$) were weighed separately using the semi-micro balance Precisa EP 225SM-DR (Scales and Measuring Instruments, Tuttlingen, DE), and the averages and variabilities of their masses were recorded. The thickness was measured using a micrometer screw Cocraft (Clas Ohlson, Insjön, Sweden) at 5 points of each shamrock – each of the hearts and the center of the shamrock. The mean and SD of the five measurements were recorded for each sample.

2.2.6.6. Mechanical properties. Mechanical properties of the films were evaluated using a Texture Analyzer Ta-XT2i (Stable Micro Systems, Godalming, UK) using a flat-faced cylindrical probe with a diameter of 2.0 mm. One shamrock clover film piece was secured between two plates using four wing screws with a cylindrical hole in the lower plate (A = 38.82 cm^2). The probe was pushed towards the film until touching (trigger force set equal to 0.05 N), and the following test speed was set to 0.1 mm/s until the breaking point (or up to the maximal displacement of 7 mm). The maximal force and the displacement of the probe at the breaking point were recorded. Puncture strength and elasticity were calculated according to the Eqs. (5) and (6).

$$Puncture\ strength = \frac{force\ to\ break}{area\ of\ the\ probe} \tag{5}$$

$$Elongation\ to\ break = \left(\frac{r_{probe} + \sqrt{a'^2 + b^2}}{r_{sample}} - 1 \right) * 100\% \tag{6}$$

where r_{sample} represents the radius of the hole in the sample holder (6.985 mm), r_{probe} is the radius of the probe (1.0 mm), $a' = r_{sample} - r_{probe}$, and b is the vertical displacement of the probe at the breaking point. The measurement was performed for five to ten replicates for each of the film formulations, at day one and twenty-one after the film preparation (e.g., one day being 24 h after drying) to capture the change of texture.

2.2.6.7. DSC. HCT, copolymers, and films were analyzed by differential scanning calorimetry (DSC) using the Differential Scanning Calorimeter DSC822e (Mettler-Toledo, Columbus, Ohio, USA) and 40 μL aluminum crucibles with punctured lids containing 4–6 mg sample. Samples were measured under a dry nitrogen gas flow of 80 mL/min. To reveal the thermal behavior of the pure drug, HCT as received was heated from 140 to 300 °C (10 K/min) after an initial equilibration at 140 °C for 2 min.

For the polymers and film formulations, the DSC method started with heating the sample from 25 °C to 180 °C, followed by equilibration for 2 min at 180 °C and cooling down to 60 °C. Thereafter, the samples were kept at 60 °C for 2 min and re-heated to 180 °C. All heating/cooling steps were performed at a rate of 20 K/min.

2.2.6.8. Raman spectroscopy. Raman spectroscopy was used to evaluate the drug distribution in the films. Films with identical composition, but without the addition of color to reduce problematic fluorescent signals, were prepared following the procedure outlined in Section 2.2.3. The spectra were acquired with the Raman spectrometer LabRAM HR Evolution (HORIBA France SAS) equipped with a 488 nm laser (50 mW), a 50 μm pin hole, a 100X objective (NA 0.9), and a theoretical spatial resolution of 330 nm. The spectra were acquired with a spatial interval of 1 μm and 3 × 5 s integration time. The focal plane was placed ca 20–30 μm into the film. The mapping sizes were 20 × 20 μm, meaning that each data set consisted of 400 spectra. The distribution of the HCT content was mapped based on the band at 1574–1617 cm^{-1}, corresponding to the aromatic ring stretching (Yadav et al., 2023). After baseline corrections of the HCT band and a band of the polymer matrix, the ratio of the integrals was calculated to avoid variation due to fluctuating laser intensity and material density. The mean and SD of the ratio of the integrals were calculated. The relative SD was used as a measure of variation in drug distribution.

2.2.6.9. Moisture content. The residual moisture in the films (12 days after preparation) was investigated by measuring the loss on drying. Films were stored at an elevated temperature (105 °C) in the oven until constant mass was achieved. The samples were weighed before (m_1) and after drying (m_2) and the mass loss (%) was calculated by Eq. (7).

$$Moisture\ content = \frac{m_2 - m_1}{m_1} * 100\% \tag{7}$$

2.2.6.10. Swelling. The swelling of the films was tested using a Petri-dish method. A piece of film was pre-weighed (m_1) (ca. 100–200 mg) and placed in a Petri dish. 5 mL of 0.01 M PBS (pH = 7.40) was prepared and added to the Petri dish. The films were allowed to swell for 5 min. Afterward, the excess liquid was gently wiped off, and the films were re-weighed (m_2). The degree of swelling was determined by Eq. (8).

$$Swelling = \frac{m_2 - m_1}{m_1} * 100\% \tag{8}$$

2.2.6.11. The pH at the surface of hydrated films. To estimate the pH of the films after hydrating in water (e.g., exerting on the mucosa), the film piece was immersed in 5 mL of water for 5 min at RT. Afterward, the pH of the aqueous media was recorded using the pH meter (Five easy F20, Mettler Toledo Inc., Columbus, OH, USA).

2.2.6.12. Disintegration. The disintegration tests were performed in 50 mL of PBS at 37 °C using the Environmental Shaker-Incubator at 60 rpm (Biosan, Riga, Latvia). A single-dose unit was placed in a beaker, and the film was visually examined. The film matrix was visually checked for potential disintegration after 15, 30, and 90 min, and the appearance was noted.

2.2.6.13. Drug release and HCT quantification. The drug release from the film was performed in small (ca. 20 mL) plastic beakers with a lid. 10 mL of 0.01 M PBS (pH 7.4) was used as the dissolution medium. A temperature-controlled shaker-incubator was set to 30 °C and 100 rpm. Film samples (approx. 100 mg film pieces) were tested under sink conditions. Samples (150 μL) were withdrawn at 2, 5, 10, 15, 20, 25, 30, 45, 60, 90, 120, 180 and 240 min, and fresh PBS was added after each withdrawal. The samples were filtered using a 0.2 μm filter, diluted with PBS if necessary, and quantified using HPLC-UV, as described below. The results were normalized to a 100 mg film piece (i.e., 1.2 mg of HCT)

to directly compare the formulations. The experiment was performed in triplicates.

The reversed-phase HPLC-UV was employed to quantify the released amount of HCT using the Novapak® C18 (4 μm; 3.9 × 150 mm) column. The mobile phase was water:acetonitrile (80:20) with a flow rate of 1.0 mL/min (isocratic elution), the oven temperature was 30 °C and the injection volume was 10 μL. The run time was 7 min and the retention time of HCT was approx. 1.9 min. The HCT was detected at the wavelength of λ = 273 nm. The HPLC-UV quantification method was checked for linearity, limit of detection, and limit of quantification in PBS. Linearity was confirmed for concentrations ranging from 0.1 to 100 μg/mL. The limit of detection was 0.16 μg/mL, and the limit of quantification was 0.48 μg/mL.

2.2.7. Cell studies

The biocompatibility and drug permeability were studied using HT29-MTX cell monolayers due to their ability to produce mucus. The cells (passage P_{25}) were cultivated at 37 °C under the 5 % CO_2 atmosphere and were passaged with the trypsin-EDTA solution when reaching 60–80 % confluence. The cell culturing medium was prepared by aseptically mixing 450 mL DMEM with 50 mL FBS, 10 mL penicillin-streptomycin, and 5 mL of NEAA, and changed three times per week.

2.2.7.14. Toxicity/biocompatibility. The toxicity of the formulations was evaluated with an MTT assay. To prepare formulations, approx. ½ of the single-dose films (about 40 % of the shamrock clover, corresponding to ca. 0.5 mg HCT) and the HCT were exposed to ultraviolet light for 30 min to inactivate potential microorganisms. These samples were soaked in 5 mL DMEM overnight at 4 °C. As a reference solution, 0.5 mg HCT in 5 mL DMEM was used. 12 parallels were tested for film formulation and reference, and 8 parallels for positive control (DMEM), negative control (1 % Triton X in DMEM) and empty wells (reference).

The cells were seeded with the initial seeding density of 2×10^4 cells/well into each well of a 96-well plate and were incubated for 24 h to attach to the surface of the well along with wells that were only filled with the DMEM to capture the background. DMEM was removed and the wells were washed twice with 200 μL of HBSS. 200 μL of the sample in the culture medium was pipetted onto each of the wells, and the plate was incubated for 2 h. Positive and negative control (DMEM and Triton X 1 %, respectively) were included. The tested samples were removed, and the wells were washed twice with HBSS before adding the MTT reagent (0.5 mg/mL in the culture medium). The well was incubated for an additional 4 h. Afterward, the wells were washed once with HBSS, and 200 μL of DMSO was added to each well. The plate was shaken at 100 rpm at RT for 15 min, protected from light, and the absorbance was evaluated on a Spectramax 190 microplate reader (Molecular Devices LLC, Sunnyvale, California, USA) using the difference between the absorbance values at 570 nm and 630 nm. The cell viability was calculated according to Eq. (9):

$$Cell\ viability = \frac{experimental\ value\ -\ negative\ control}{positive\ control\ -\ negative\ control} * 100\% \quad (9)$$

2.2.7.15. Permeability. The permeability experiment was carried out using 6-well plates with the Transwell® inserts (Costar, Corning, New York, USA) with a 0.4 μm pore size and a growing area of 4.2 cm^2 with an initial seeding density of 2.4×10^4 cells/cm^2. The cells were cultured on the membrane surface for 22 days before conducting the experiments.

For the permeability experiment, the film pieces and the reference (HCT dissolved in HBSS) with a target content of HCT of approx. 225 μg per well (1.5 mL) to ensure sink conditions were used. The DMEM media was removed from the donor and acceptor compartment, and the monolayers of cells and wells were washed twice with HBSS, before 2.5 mL and 1.5 mL of fresh HBSS were added to the donor and acceptor compartment, respectively. Samples of 200 μL were taken from the acceptor cell after 30, 60, 120, 180 and 240 min and replaced with warm HBSS. The drug in the acceptor chamber at each time point was quantified by UV–VIS spectrometry at the wavelength λ = 273 nm.

The flux (J) was calculated as in Eq. (10), where dQ represents the amount of drug permeated through the membrane, A is the Transwell surface area, and dt is the time.

$$J = \frac{dQ}{A\ x\ dt} \quad (10)$$

To check the integrity of the mucus-covered cell monolayer after the incubation with the formulations, a CF solution (20 μM) was added to the donor compartment after removing film residues and washing with HBSS. After 1 h of incubation, the amount of CF that had permeated into the acceptor cell was evaluated using the fluorometer Fluoroskan (Thermo Fischer Scientific Instruments Co., Ltd., Shanghai, China).

The integrity of the cell monolayer was additionally monitored by measuring the transepithelial electrical resistance (TEER) using a Millicell® ERS-2 Voltohm meter (Millipore Co, Bedford, MA, USA) before, during, and after the permeability experiment to detect potential disruption of the monolayer and was normalized by the Transwell insert surface area.

2.2.8. Statistical analysis

The statistical differences (post-hoc ANOVA, t-test) were performed when applicable.

3. Results and discussion

3.1. Characterization of the copolymers

Understanding the compositions, structures, and properties of the PVA/PVAc copolymers is crucial for developing new SSE formulations and thus achieving the desired final product properties. This was combined with determining relevant polymer concentrations and printing settings for SSE to achieve films with suitable mechanical properties and evaluating the effect of polymers on the film formulations.

The copolymers were characterized to determine their chain size and composition of the polymer chains. Table 2 shows that the PVA88 and PVA98 had similar molecular weights and hydrodynamic radii. The intrinsic viscosity and hydrodynamic radius were somewhat higher for PVA98 than PVA88, indicating that PVA98 chains expand to a higher degree in contact with water. It should be noted that the SEC method was not suitable for the determination of the properties of PVA35, PVA50 and PVA74 due to incomplete solubilization of the polymer in the mobile phase, therefore the data for these copolymers could not be obtained.

The viscosity of the 10 % w/V polymer dispersion in water varied from 2.5 to 27.0 mPa × s as shown in Table 2, following the same order of averages of the stated manufacturer's viscosities for a 4 % solution in water at 20 °C (see Table 1). Lower viscosity values for PVA35 and

Table 2
Determined properties of the PVA/PVAc copolymers: molecular weight (Mw), hydrodynamic radius (R_h), intrinsic viscosity, viscosity of 10 % w/V polymer in water, and degree of hydrolysis.

	Mw (kDa)	R_h (nm)	Intrinsic viscosity (mL/g)	Viscosity (mPa × s) (mean ± SD)	Degree of hydrolysis (%)
PVA35	n/a[1]	n/a	n/a	2.5 ± 0.0[1]	33 %
PVA50	n/a	n/a	n/a	5.6 ± 0.0[1]	48 %
PVA74	n/a	n/a	n/a	24.2 ± 2.8[2]	74 %
PVA88	24	5.5	39	14.0 ± 0.1[2]	87 %
PVA98	23	5.7	41	16.1 ± 0.2[2]	98 %

n/a: the results could not be obtained by the used method.
[1] Determined at the speed of 200 rpm.
[2] Determined at the speed of 100 rpm.

Table 3
Detailed information about copolymers, obtained by ^{1}H NMR.

	Acetate protons	Methylene protons	(OH, OH)	(OH, OAc)	(OAc, OAc)	n_{OH} [1]	n_{Oac} [2]
PVA35	0.50	0.50	0.30	0.16	0.54	4.2 (1.5)	8.3 (2.6)
PVA50	0.44	0.56	0.39	0.16	0.44	6.0 (2.0)	6.5 (2.0)
PVA74	0.28	0.72	0.72	0.1	0.18	14.8 (3.5)	5.2 (1.4)
PVA88	0.16	0.84	0.81	0.1	0.08	17.5 (6.0)	2.5 (1.1)
PVA98	0.03	0.97	n/a	n/a	n/a	n/a	n/a

[1] The average lengths of VA blocks were determined experimentally, with the average length for the random copolymer provided in parentheses.
[2] The average lengths of VAc blocks were determined experimentally, with the average length for the random copolymer provided in parentheses.

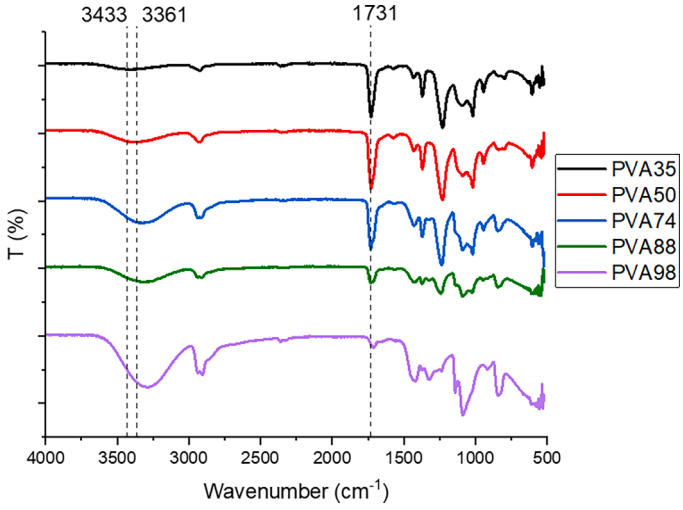

Fig. 3. ATR-FTIR spectra of the copolymers.

PVA50 were expected, as these copolymers did not dissolve fully in water at this concentration; rather, they formed an opaque, colloidal dispersion. These results can be related to their difference in hydrophilicity, with PVAc and PVA being non-polar and polar polymers, respectively (Squillace et al., 2020). The more polar copolymers with a higher VA proportion in water may be able to expand more in contact with water by forming inter- and intra-molecular hydrogen bonds (Briscoe et al., 2000). Despite the fact that Mw could not be obtained for PVA35, PVA50 and PVA74, it may be assumed that PVA74 has a higher Mw than other copolymers. The viscosity is a vital parameter for a successful SSE, where polymers are often used as thickening agents to achieve suitable solid content or to optimize product properties and performance accordingly (Govender et al., 2021).

The composition of polymers was studied by ^{1}H NMR, and the results are shown in Table 3. NMR spectra are available in Supplementary material, Fig. S1. The obtained results showed that the degree of hydrolysis was in good agreement with the supplier (within two percent of the values provided). The average length of blocks with repeating monomers of VA or VAc for PVA50 was around 6 units, compared to 2 units for random copolymer (Table 3). This shows that these copolymers had repeating monomers distributed in blocks to some degree, rather than monomers randomly distributed along the polymeric chain. This can have an influence on both the solubility of the polymer itself, how it associates, as well as how it interacts with co-solubilized drugs in the wet film formulation and final film.

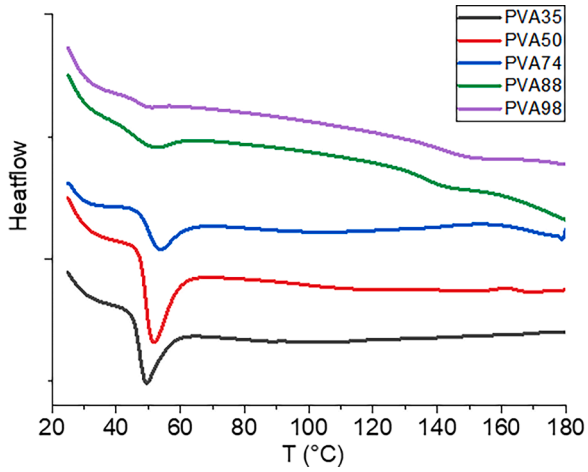

Fig. 4. DSC curves of the pure copolymers.

ATR-FTIR was also used to characterize the copolymers. The acetyl group had a clear peak at around 1731 cm^{-1} due to the stretching of C=O and C—O from acetate (Mansur et al., 2008), as can be seen in Fig. 3. This IR peak increases with increased VAc proportion. The IR peaks corresponding to the vibration of the hydroxyl groups had a broad stretching band around 3389 cm^{-1} to 3281 cm^{-1} for PVA98 to PVA35, suggesting intra- and intermolecular hydrogen bonds among the hydroxyl groups (Mansur et al., 2008; Qureshi et al., 2021). The results are in agreement with a shift of the minima towards higher wavenumbers with the increasing proportion of alcohol groups for PVA/PVAc (Isasi et al., 1994). In addition, a careful inspection of PVA50 shows an IR peak at the wavelength 3361 cm^{-1}. In the literature, it has been shown that multiblock PVA/PVAc chains with DH equal to 52 % have a similar shift (3375 cm^{-1}), whereas more random chains had their peak at 3433 cm^{-1} (Merekalova et al., 2017). This observation aligns with the NMR findings, indicating that the polymer exhibits a block distribution of monomers rather than a random distribution.

The DSC curves of the copolymers are shown in Fig. 4. The glass transition temperatures (T_gs) were found to be between 50 and 54 °C for the five copolymers, and the size of this peak generally increased with higher proportions of VAc in the polymer. Large enthalpy recoveries were seen for the measured T_gs for PVA35, PVA50 and PVA74. The measured T_gs for these three copolymers were in line with reported values for multiblock PVA/PVAc polymers, while comparable copolymers with the same monomer ratios, although distributed randomly, have been reported to have T_gs in the range of 63 to 70 °C (Ilyin et al., 2014). This is another indication that these copolymers do indeed have their monomers distributed in blocks.

PVA/PVAc copolymers have been described to self-assemble, giving colloidal aggregates in the nanometer range in aqueous solution as a result of intermolecular paracrystalline domains, hydrogen bonds, and/or by hydrophobic interactions between vinyl acetate sequences of the

Table 4
Average particle size (D_v) and volume contribution (V) of 1 % w/V polymers in mQ water (mean ± SD) for the main peak (A) and the second largest contributing peak (B).

	D_{vA}(nm)	V_A (%)	D_{vB} (nm)	V_B (%)
PVA35	43.0 ± 0.2	99.4 ± 0.2	/	/
PVA50	27.7 ± 0.3	99.0 ± 0.2	/	/
PVA74	36.2 ± 0.5	80.9 ± 5.3	630 ± 137	13.8 ± 4.7
PVA88	13.4 ± 0.3	87.8 ± 1.3	390 ± 23	8.4 ± 1.4
PVA98	13.7 ± 0.2	86.7 ± 3.1	420 ± 79	10.4 ± 2.8

copolymer (Atanase and Riess, 2010). It is reasonable to expect stronger intermolecular hydrophobic interactions in water for the copolymers with higher VAc proportion. The particle size and volume fractions of the aggregates are shown in Table 4. The sizes of the clusters are important and can contribute to understanding the solvation mechanism of the polymer chains in the aqueous media. Copolymers with the highest fraction of VAc units have been suggested to form pseudo-micelles. Several solvated hydrophilic alcohol chains are organized into a loop, forming an outer shell with the hydrophobic acetate parts of the chain located in a core, thereby reducing their contact with the polar solvent. This increases the hydrodynamic radius (Budhlall et al., 2003). Our observations are in line with this, as the copolymers with the highest proportion of VAc chains have the highest average diameter (D_{v1}) in water. If a hydrophobic drug is distributed to the hydrophobic core, it could be expected to slow down the drug release process. PVA88 and PVA98 had the lowest D_{v1}; with the lowest proportion of acetate groups (Budhlall et al., 2003). The diameter values obtained by DLS are comparable with radius values obtained by SEC (see Table 2), indicating that the DLS maps single chains. PVA74, PVA88 and PVA98 have an additional larger peak, which could be attributed to scattering of impurities in the sample.

3.2. Formulation composition and semi-solid extrusion

The formulations' composition was based on the solubility of polymers and HCT in the chosen solvent. The solubility of HCT in water at RT was 0.7 mg/mL and increased with increasing proportion of ethanol. At the same time, water was a suitable solvent for the polymers with a higher VA proportion but formed an opaque solution for the copolymers with a higher proportion of VAc. Ethanol and methanol were suitable solvents for the copolymers with a higher VAc proportion but resulted in precipitation of PVA88 and PVA98. As a compromise, a water/ethanol 1:1 (v/v) mixture was used where HCT dissolved easily (7 mg/mL) and up to 40 % (w/V) of the copolymers could be dissolved, except for PVA98, which precipitated in this solvent mixture. Therefore, half the concentration of both PVA98 and the drug was used in this formulation to obtain the same drug/polymer ratio in the resultant dry films.

To obtain visually acceptable films with high reproducibility using semi-solid extrusion (SSE), the formulations should possess a suitable viscosity (Govender et al., 2021). The wet film formulations had a wide range of dynamic viscosity values (see Supplementary material, Table S1), where the higher VA proportion resulted in a larger expansion of the polymer chains in a 1:1 water/ethanol (v/v) mixture. A direct comparison of the viscosities for PVA98 and the other copolymers cannot be made due to the different polymer concentrations. In general, SSE resulted in films with the desired designed shamrock shape with clearly defined clovers (see Fig. 2). However, printed films with PVA35 and PVA50 showed small zones of less extruded material, resulting in gaps in the films and less sharp edges compared to the other printed films. This was likely due to the lower viscosities of the PVA35 and PVA50 solutions, causing the material to unintentionally drip from the nozzle before and during printing, resulting in less material being deposited in some places. In addition, the lower viscosity of the solutions allowed them to flow slightly on the printing surface after deposition, leading to less sharp edges. Although these effects were only observed upon thorough inspection and comparison with other printed films, the results indicate that these viscosities, i.e., 154 and 178 mPa × s, were likely slightly below what should be recommended to use in this SSE set-up, while viscosities from 516 to 2991 mPa × s were deemed suitable.

3.3. Physical and mechanical characteristics of the printed films

After leaving the films to dry overnight, the PVA74, PVA88, and PVA98 films were easily peeled off the printing surface – the latter two started to detach from the printing surface already during the drying process. PVA35 and PVA50 films were more challenging to remove, as they were sticking to the surface and were prone to break during the removal. The hydrophobic nature of the printing surface (Bench surface protector) may have provided a more favorable contact angle for the more hydrophobic copolymers, whereas the printing surface repelled the more hydrophilic ones.

SSE resulted in a relatively good mass uniformity of the shamrocks (< 5 % relative SD), due to the precise application of the formulation onto the printing surface (see Table 5). Printing with formulations with lower viscosities (the PVA35 and 50) did not appear to affect the average mass variation of the resulting films (396 to 441 mg), except for the PVA98 films, which had a lower mass likely due to the lower polymer concentration in the wet film formulation. The thickness of the films varied at different points of the same film piece. This can be attributed to the extrusion process, where certain areas of the film experienced multiple material depositions due to the designed shape, leading to discrepancies compared to other areas.

The films' residual moisture content after equilibration in the moisture chamber (day 12, approx. 33 % RH) varied from 3.2 to 6.7 % (see Table 5), where the films with a higher proportion of VA contained more moisture. Statistically, it could be shown that PVA35 and PVA50 contained less moisture than other films, and PVA74 contained less moisture than PVA98 ($p < 0.05$). The results suggest that a higher proportion of hydrophilic VA groups facilitated the capture of water, which could affect the films' mechanical properties, as well as the physical and chemical stability of some APIs.

From a pharmaceutics perspective, to be relevant, the films require adequate robustness, which is often evaluated with mechanical tests (Preis et al., 2013). The mechanical properties of the films are presented in Table 5. None of the films were punctured using our standard probe ($r = 3.52$ mm), therefore a narrower probe ($r = 1$ mm) was used. Freshly prepared films based on PVA35 and PVA50 were not punctured under the performed conditions immediately after drying at ambient conditions (day 1), and thus the elongation to break could not be calculated for these copolymers. The puncture strength of the films increased with increasing VA proportion from PVA74 to PVA98. It should be noted that PVA98 films had the lowest thickness, but the largest puncture strength. Despite the fact that PVA35 and PVA50 were not punctured, they appeared brittle and were easier to break by folding. The elongation to break reached the highest values for PVA74 and PVA88, which were also the most robust polymers and appeared easiest to handle. The effect of residual moisture on mechanical properties was evaluated after equilibration of the films in a moisture chamber (approx. 33 % RH). After 21 days of storage, all the films were punctured under the performed

Table 5
Properties of the films printed from the copolymers (mean ± SD), where n is the number of replicates.

	Film mass (mg), $n \geq 8$	Film thickness (mm), $n \geq 8$	Moisture content (day 12) (%), $n = 3$	Puncture strength (day 1) (N/mm^2), $n \geq 5$	Elongation to break (day 1) (%), $n \geq 5$
PVA35	404 ± 4	0.24 ± 0.07	3.2 ± 0.2	n/a[1]	n/a
PVA50	396 ± 20	0.24 ± 0.08	3.2 ± 0.2	n/a	n/a
PVA74	441 ± 8	0.30 ± 0.09	5.8 ± 0.2	4.6 ± 0.1	42.0 ± 2.2
PVA88	438 ± 9	0.32 ± 0.12	6.1 ± 0.2	7.0 ± 0.6	34.8 ± 8.0
PVA98	252 ± 10	0.18 ± 0.07	6.7 ± 0.4	9.4 ± 0.9	14.3 ± 2.8

[1] n/a., stand for *not applicable,* and in this study, it was due to that the films did not break under the tested conditions (1 mm probe with maximal force of 5 kg).

conditions (see Supplementary material, Table S2). PVA35 and PVA50 became more brittle during the storage process. PVA74 and PVA88 had increased puncture strength and only smaller changes in elasticity. PVA98 became more brittle than other formulations and lost some elasticity. Chen et al. have shown that differences in mechanical properties might be attributed to the monomer ratio and residual water (Chen et al., 2008), which was in accordance with our results, as films with a higher proportion of PVOH also showed higher residual water and were more elastic. The findings after storage (21 days at 33 % RH) suggest that the rest moisture content in the films was reduced as compared to the freshly prepared films (day 1). The product performance could be adjusted accordingly by optimizing the printing parameters where an increased layer height would increase the thickness and puncture strength of the films. This could be relevant for PVA35 and PVA50, compensating to some degree for their brittleness, whereas the stronger and more elastic PVA74, PVA88 and PVA98 could be processed into thinner films and still be easy to handle.

3.4. Solid state properties of the films

3.4.1. DSC

DSC was employed to identify the solid state of HCT in the films and to check for potential crystalline areas of the polymer after film preparation. As the polymers started to degrade at the onset of melting of HCT at 269 °C (see Supplementary material, Fig. S2 and S3), it was not possible to identify the melting of HCT in the films (data not shown). The DSC curves of the freshly prepared films are shown in the Supplementary material, Fig. S4. An endothermic peak of 100–110 °C was visible for freshly prepared PVA35 and PVA50 films. In the literature, HCT has been found to have a glass transition temperature at 110 °C (Alzghoul et al., 2014). This endothermic peak was attributed to the polymer, as it also appeared in control films without HCT and could be the result formation of small crystals of polymer during drying. No such sharp peaks were detected for films based on PVA74, PVA88 and PVA98, indicating that the core-shell nanostructure observed with DLS for PVA35 and PVA50 might be preserved and form phase-separated structures that could crystallize.

3.4.2. Raman spectroscopy

Raman spectroscopy was used to evaluate the drug distribution within the film on a micrometer level. The spectra acquired with a 488 nm laser gave clear bands with little fluorescence for the non-colored films. The HCT band at 1574–1617 cm^{-1} corresponding to the aromatic ring stretching (Yadav et al., 2023) was clearly differentiated and was not overlapping with VAc or VA, while the band at 1688–1754 cm^{-1} corresponding to the carbonyl stretching (Taylor et al., 2001) belongs to VAc (see Fig. 5). Therefore, the ratio of the two bands was used to determine the relative concentration of HCT. Additional indications of HCT in the film were the bands at 1166–1173 cm^{-1} and 1285–1303 cm^{-1}. For films based on PVA98, the carbonyl stretching was too weak, and the band at 1397–1463 cm^{-1} (CH_2 bending of PVA) (Badr et al., 2004) was used for the calculations.

The relative SD of the integrals of the HCT and VAc at different locations ranged between 3.7 and 7.9 % for all samples (see Supplementary material, Table S3), which indicates that the drug was evenly distributed within the polymeric matrix at a micrometer level film for all copolymers. There was no indication on this length scale of potential phase separation for copolymers or crystal formations that would lead to uneven drug distribution within the films. Raman heat map for PVA50 is shown in Fig. 6 and for all the copolymers in the Supplementary material (Fig. S5).

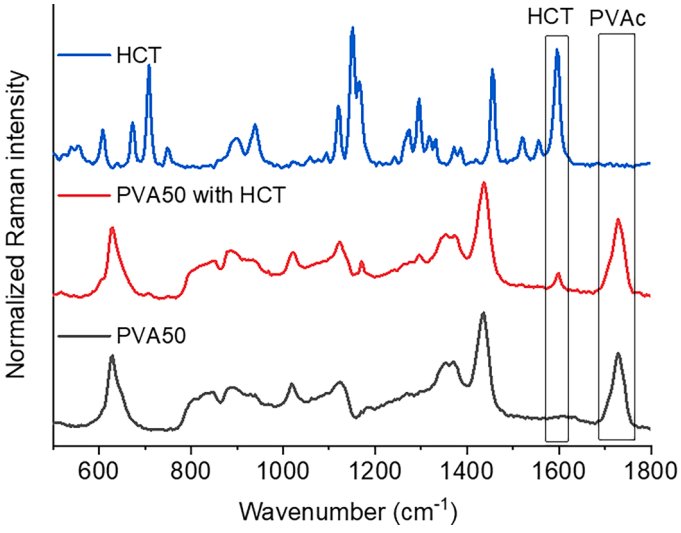

Fig. 5. Example of a normalized Raman spectra of HCT, PVA50 with HCT (film) and PVA50. The aromatic stretch of HCT at 1574–1617 cm^{-1} and carbonyl stretching of VAc at 1688–1754 cm^{-1} are marked with a box.

3.5. Swelling, disintegration and drug release

The following chapter focuses on the behavior of the films when exposed to the aqueous media, where drug release takes place. The swelling of the films is presented in Table 6. All films, except for PVA98, demonstrated a comparable range of swelling ratios (averaging from 86 % to 136 %), with no statistically significant differences observed between them ($p > 0.05$). PVA98 swelled significantly more than other formulations, which could result from the lower thickness and mass of PVA98 films (lower polymer concentration) leading to an increased relative surface area to volume ratio and/or higher hydrophilicity.

The average surface pH of the swollen films ranged between 5.81 and 6.46 (see Table 6), while the pH of a 5 mg/mL HCT solution in 50 % ethanol/water was 5.25. Relatively neutral pHs of these formulations are expected with respect to the components present in the films, and to reported values, as PVA should have a pH of 4.5–6.5 (pH. *Eur. 11.2*, 2023)

The disintegration of the films in PBS was evaluated visually under agitation in a beaker on a shaker-incubator (37 °C) to explore the films' suitability for different drug delivery applications. The films based on PVA35 and PVA50 started to disintegrate after 15 min, and the matrix tended to form a gel in a form of "polymer clumps" that stuck to the bottom of the beaker. The films based on PVA74 and PVA88 also started

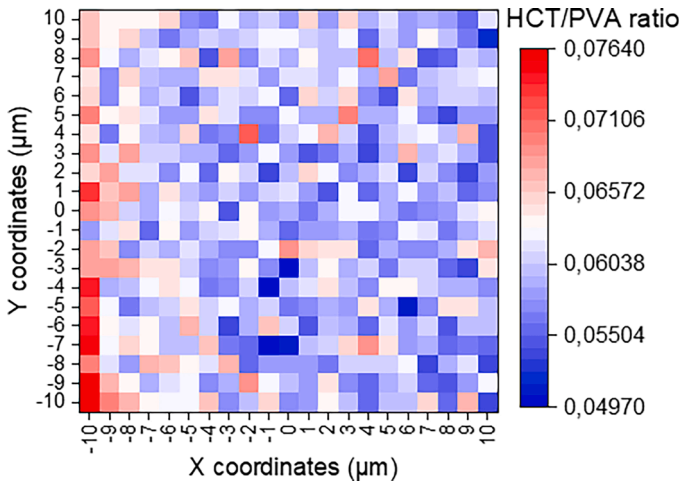

Fig. 6. Example of a 20 × 20 μm^2 Raman heat maps for PVA50. The figure represents the ratio of HCT Raman bands (1688–1754 cm^{-1}) and PVAc (1397–1463 cm^{-1}). The small variation in HCT/PVA ratio (relative SD of 7.1 %) indicates that no phase separation has occurred.

Table 6
Swelling and surface pH of the films (mean ± SD). The number of replicates is equal to 3.

	Swelling (%)	pH
PVA35	86 ± 17	6.46 ± 0.06
PVA50	118 ± 70	6.05 ± 0.06
PVA74	136 ± 19	5.81 ± 0.03
PVA88	94 ± 8	5.88 ± 0.02
PVA98	365 ± 127	5.89 ± 0.03

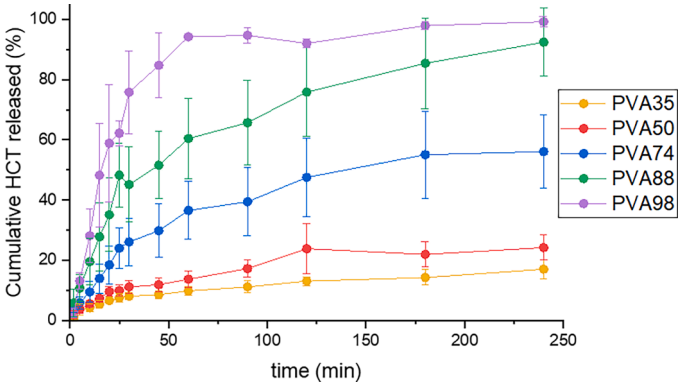

Fig. 7. HCT total release (sink conditions), normalized per a 100 mg film piece ($n = 3$). The values are presented as average ± standard deviation.

to disintegrate after 15 min and were completely disintegrated after 30 min, with only smaller fragments floating around in the media. The films based on PVA98 remained relatively intact during the first 15 min, but started to disintegrate after 30 min, with no coherent matrix seen at the end of the experiment (90 min).

The drug release is presented in Fig. 7. The polymer composition strongly influenced the HCT release from the films, where the drug release rate increased with increasing VA proportion. The t_{50}, the time when 50 % of the drug was released, appeared after approx. 12 min, 45 min, and 180 min for the PVA98, PVA88 and PVA74, respectively, and was not achieved for the PVA35 and PVA50 after 4 h of the drug release study. The slower drug release for these copolymers might be attributed to the more hydrophobic nature of these copolymers, which could form micelle-like structures (see Section 3.1). The larger block areas of PVAc could enable the formation of hydrophobic interactions between acetate groups and hinder access to the dissolution media. The hydrophobic VAc groups might also interact with HCT, especially for the copolymers that have a more block-wise distribution of the monomer units (see Table 3). The higher PVA proportion in PVA98 provided an almost complete release of the drug within 60 min. The high degree of swelling for PVA98 may have contributed to an increased drug release rate at the beginning, allowing the dissolution media to penetrate the film, hydrate the polymer, and dissolve the HCT, resulting in a faster drug release. The other formulations were hydrated and released the drug more slowly, providing a sustained drug release over several hours, or as indicated, days.

It is of note that the drug release rate of the drug was not in accordance with the disintegration tests done on the same films. PVA35, PVA50 and PVA74 showed drug release over multiple hours after full disintegration of the films. This suggests that these films retain the drug within their undissolved matrix while exhibiting slow disruption of the film structure with time. If used for oral drug delivery, this could prove advantageous, as it would be possible to adjust the release rate by using copolymers with different monomer ratios. However, the relatively rapid disintegration coupled with slow release could be undesirable for buccal delivery, as the films would disintegrate in the buccal cavity. Films intended for buccal absorption might need an additional layer to conserve the film structure after swelling in water or copolymers with larger molecular weight to slow down the disintegration.

3.6. Cell studies

As the copolymers used were not of a pharmaceutical grade and are approved by the US Food and Drug Administration (FDA), for example in foods as outlined in the Federal Register (21 CFR) (Food and Drug Administration, 2022), cell studies on a mucus-producing HT29-MTX cell line were included to evaluate the films' biocompatibility. In addition, HCT permeability through cell monolayers was investigated. In the literature, it has been shown that higher polymer concentration leads to increased toxicity (Prasad et al., 2014).

Permeability studies of HCT from the films through a cell monolayer were employed to understand the effect of the formulation on the permeation through the membrane. Since some of the polymers seemed to retain the drug in the film preventing the drug release, it was relevant to investigate whether this effect would also directly influence permeability.

Fig. 8 shows the flux of HCT through the monolayer, where the HCT flux from the PVA35 and PVA50 films was significantly lower than for the formulations with a highest proportion of VA ($p < 0.05$). These results suggest that the monomer ratio and/or the blocky distribution of VA and VAc units in the polymer chains had an impact on the permeability. The differences in flux can be related to the drug release results observed in Section 3.5, where the higher proportion of VAc retained the HCT, and slowed the release of the drug by the formation of a mechanically stronger gel (Boateng et al., 2012). The flux of HCT dissolved in HBSS was higher than the HCT incorporated in films, since the drug was already dissolved and available for permeation, and no prior release was needed from the matrix.

The amount of formazan formed from the dye MTT is an indicator of the metabolic activity of the cells and is often used to assess the potential toxicity of the formulations. Films based on PVA35 and PVA88 showed cell viability values were close to 100 % (see Supplementary material, Fig. S6). The calculated cell viability for PVA50 and PVA74 was higher (140 ± 19 % and 124 ± 18 %, respectively) and lower for PVA98 (76 ± 15 %). The cell viability above the referential values of 100 % could be a result of cell irritation, as MTT is prone to compounds that interfere with cell metabolic activity. However, the regulatory requirements set 30 % of cell metabolic activity reduction as a sign of potential toxic effects on the cells (Kozlovskaya et al., 2015), and none of the formulations

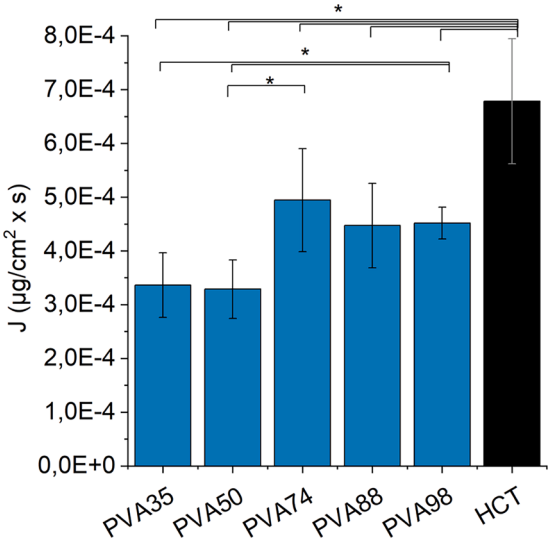

Fig. 8. Flux (J) of HCT in the formulations and the reference ($n = 4$). Values are presented as average ± standard deviation. Formulations encompassed by a common bracket with asterisk are significantly different from each other ($p < 0.05$).

exceeded this limit.

Biocompatibility was additionally estimated with the measurement of TEER and CF permeation. TEER values were generally stable throughout the experiment indicating an intact barrier (Supplementary material, Fig. S7). The amount of CF permeated through the monolayer after incubation with the formulations ranged from 1.6 to 1.9 % (Supplementary material, Fig. S8), was in the same range as the reference (1.7 %), and was considered low compared to previous studies with the same method (Korelc et al., 2023). Stable TEER values and low CF permeability in combination with the cell viability tests indicate good biocompatibility of the formulations.

3.7. Selecting the optimal monomer ratio for SSE

The main factors influencing the formulation preparation and processing were the solubility of the copolymers, their hydrophobicity, and the viscosity of the film formulations, and will be further summarized below.

- *The solubility of the polymers*: polymers with a higher VA proportion were more likely to dissolve in water, while polymers with a higher proportion of VAc were more likely to dissolve in ethanol. The suitable solvent should be chosen based on the monomer ratio as well as the drug solubility properties for the co-dissolution of polymer and drug.
- *Hydrophobicity of the polymers*: the more hydrophobic polymers were likely to stick to the printing surface with similar properties, and the resulting films were brittle and difficult to remove. If choosing specific copolymers to work with, the printing surface could be changed so that the resulting films would be easier to remove.
- *Suitable viscosity range*: too low viscosity can result in a non-uniformly extruded gel and unintentional dripping from the nozzle, leading to discrepancies in thickness throughout the film piece. Too high viscosity, on the other hand, can clog the nozzle, and prevent extrusion of material. The viscosities in ethanol/water were strongly dependent on the monomer ratio, increasing with the increased VA proportion. In the tested set-up, the most suitable viscosity values were deemed in the range 516 – 2991 mPa $\times$ s.

The main effects of the monomer ratio on the properties of the formulation were differences in easiness to handle, mechanical properties, drug release and permeability, and are summarized below.

- *Handling*: films made with copolymers with a higher VA proportion were easier to peel off the printing surface, and appeared stronger and more elastic. The biggest differences were observed between 35 and 50 % VA and 74–98 % VA proportion.
- *Mechanical properties*: films with 35 and 50 % VA did not break under the performed setup and were relatively strong and rigid. Films with 74–98 % VA broke under the performed conditions.
- *Drug release and permeability*: the HCT release rate from the films was faster from the more hydrophilic copolymers, and decreased with the increasing VAc proportion. The drug release affected the flux of the drug through the cell monolayer. Copolymers with a higher acetate proportion could be used for sustained drug delivery systems.

SSE settings can be used to tune the printed shape, layer height, width, and gel consistency/extrusion percentage. By increasing the layer height, a larger amount of material is deposited onto the printing surface, leading to a thicker film and higher drug load per surface area. This would increase the dose, however, it would also impact the rate of release and mechanical properties. By utilizing different monomer ratios, tuning of release rate and mechanical properties can be achieved without impacting the total dose. By incorporating PVA/VAc in the film formulations, more flexibility and potential parameters for personalization are possible for drug delivery systems using SSE.

4. Conclusion

Drug delivery properties can be tailored by using the copolymer PVA/PVAc with different monomer ratios. The monomer ratio affects the formulation process, including wet film formulation preparation, semi-solid extrusion process and properties of prepared films. SSE with more viscous wet film formulations with higher VA proportions was easier, and films were elastic and easy to handle. On the other hand, films with higher VAc proportion were more brittle and less elastic after drying. The hydrophobicity of copolymers with a higher VAc proportion played a role in a slower release rate of HCT and lower flux rate over cell monolayer compared to copolymers with a higher proportion of VA. This study highlights the importance of choosing the correct monomer ratio of PVA/PVAc copolymers for the desired application. The possibility of using all these copolymers in SSE provides a promising potential in the development of personalized drug delivery systems.

CRediT authorship contribution statement

Karin Korelc: Conceptualization, Methodology, Investigation, Data curation, Formal analysis, Writing – original draft, Visualization. **Bjarke Strøm Larsen:** Conceptualization, Methodology, Investigation, Data curation, Writing – review & editing. **Anna-Lena Heintze:** Methodology, Investigation, Data curation, Formal analysis, Writing – review & editing. **Åke Henrik-Klemens:** Methodology, Investigation, Data curation, Formal analysis, Writing – review & editing. **Jakob Karlsson:** Methodology, Investigation, Data curation, Formal analysis, Writing – review & editing. **Anette Larsson:** Methodology, Supervision, Investigation, Data curation, Writing – review & editing, Project administration. **Ingunn Tho:** Conceptualization, Resources, Methodology, Writing – review & editing, Supervision, Funding acquisition, Project administration.

Declaration of Competing Interest

The authors declare that they have no known competing financial interests or personal relationships that could have appeared to influence the work reported in this paper.

Data availability

Data will be made available on request.

Acknowledgement

This project was carried out as part of Nordic POP (Patient Oriented Products), a Nordic University Hub funded by NordForsk (project number 85352). Åke Henrik-Klemens was supported by the "FibRe—a Competence centre for Design for Circularity: Lignocellulose-based Thermoplastics", partly funded by the Swedish Innovation Agency VINNOVA (Grant No. 2019–00047). The help and support in the laboratory from Ivar Grove, Bente Breiby and Tove Larsen is greatly appreciated. The cell line HT29-MTX was kindly provided by Dr. Thécla Lesuffleur (INSERM UMR S 938, Paris, France). The authors would like to acknowledge Kuraray Poval for providing PVA/PVAc copolymers.

Supplementary materials

Supplementary material associated with this article can be found, in the online version, at doi:10.1016/j.ejps.2023.106645.

References

Alzghoul, A., Alhalaweh, A., Mahlin, D., Bergström, C.A.S., 2014. Experimental and computational prediction of glass transition temperature of drugs. J. Chem. Inf. Model. 54, 3396–3403. https://doi.org/10.1021/ci5004834.

Atanase, L.I., Bistac, S., Riess, G., 2015. Effect of poly(vinyl alcohol-co-vinyl acetate) copolymer blockiness on the dynamic interfacial tension and dilational viscoelasticity of polymer-anionic surfactant complex at the water-1-chlorobutane interface. Soft Matter 11, 2665–2672. https://doi.org/10.1039/c4sm02766c.

Atanase, L.I., Riess, G., 2010. Poly(vinyl alcohol-co-vinyl acetate) complex formation with anionic surfactants particle size of nanogels and their disaggregation with sodium dodecyl sulfate. Colloids Surf. Physicochem. Eng. Asp. 355, 29–36. https://doi.org/10.1016/j.colsurfa.2009.11.024.

Badr, Y.A., Abd El-Kader, K.M., Khafagy, R.M., 2004. Raman spectroscopy study of CdS, PVA composite films. J. Appl. Polym. Sci. 92, 1984–1992. https://doi.org/10.1002/app.20017.

Boateng, J.S., Matthews, K.H., Auffret, A.D., Humphrey, M.J., Eccleston, G.M., Stevens, H.N., 2012. Comparison of the *in vitro* release characteristics of mucosal freeze-dried wafers and solvent-cast films containing an insoluble drug. Drug Dev. Ind. Pharm. 38, 47–54. https://doi.org/10.3109/03639045.2011.590496.

Briscoe, B., Luckham, P., Zhu, S., 2000. The effects of hydrogen bonding upon the viscosity of aqueous poly(vinyl alcohol) solutions. Polymer 41, 3851–3860. https://doi.org/10.1016/S0032-3861(99)00550-9 (Guildf).

Budhlall, B.M., Landfester, K., Sudol, E.D., Dimonie, V.L., Klein, A., El-Aasser, M.S., 2003. Effect of poly(vinyl alcohol) molecular architecture on aqueous phase conformation. Macromolecules 36, 9477–9484. https://doi.org/10.1021/ma030027d.

Cano, A.I., Cháfer, M., Chiralt, A., González-Martínez, C., 2015. Physical and microstructural properties of biodegradable films based on pea starch and PVA. J. Food Eng. 167, 59–64. https://doi.org/10.1016/j.jfoodeng.2015.06.003.

Chen, J., Liu, C., Chen, Y., Chen, Y., Chang, P.R., 2008. Structural characterization and properties of starch/konjac glucomannan blend films. Carbohydr. Polym. 74, 946–952. https://doi.org/10.1016/j.carbpol.2008.05.021.

El Aita, I., Rahman, J., Breitkreutz, J., Quodbach, J., 2020. 3D-Printing with precise layer-wise dose adjustments for paediatric use via pressure-assisted microsyringe printing. Eur. J. Pharm. Biopharm. 157, 59–65. https://doi.org/10.1016/j.ejpb.2020.09.012.

Fernandes, G., de, J.C., Campelo, P.H., de Abreu Figueiredo, J., Barbosa de Souza, H.J., Peixoto Joele, M.R.S., Yoshida, M.I., Henriques Lourenço, L., de, F., 2022. Effect of polyvinyl alcohol and carboxymethylcellulose on the technological properties of fish gelatin films. Sci. Rep. 12, 10497. https://doi.org/10.1038/s41598-022-14258-y.

Food and Drug Administration, 2022. Indirect food additives: polymers. URL https://www.ecfr.gov/current/title-21/chapter-I/subchapter-B/part-177 (accessed 10.08.2023).

Gkaragkounis, A., Fatouros, D.G., 2023. Nano- and microfabrication techniques in drug delivery: semi-solid extrusion 3D printing for the development of dosage forms for special patient groups, 125–136.

Govender, R., Kissi, E.O., Larsson, A., Tho, I., 2021. Polymers in pharmaceutical additive manufacturing: a balancing act between printability and product performance. Adv. Drug Deliv. Rev. 177, 113923 https://doi.org/10.1016/j.addr.2021.113923.

Gumieniczek, A., Galeza, J., Mroczek, T., Wojtanowski, K., Lipska, K., Pietras, R., 2018. Kinetics and characterization of degradation products of dihydralazine and hydrochlorothiazide in binary mixture by HPLC-UV, LC-DAD and LC–MS methods. Chromatographia 81, 1147–1162. https://doi.org/10.1007/s10337-018-3555-8.

Ilyin, S.O., Malkin, A.Y., Kulichikhin, V.G., Denisova, Y.I., Krentsel, L.B., Shandryuk, G. A., Litmanovich, A.D., Litmanovich, E.A., Bondarenko, G.N., Kudryavtsev, Y.V., 2014. Effect of chain structure on the rheological properties of vinyl acetate-vinyl alcohol copolymers in solution and bulk. Macromolecules 47, 4790–4804. https://doi.org/10.1021/ma5003326.

Isasi, J.R., Cesteros, L.C., Katime, I., 1994. Hydrogen Bonding and sequence distribution in poly(vinyl acetate-co-vinyl alcohol) copolymers. Macromolecules 27, 2200–2205. https://doi.org/10.1021/ma00086a033.

Johannesson, J., Khan, J., Hubert, M., Teleki, A., Bergström, C.A.S., 2021. 3D-printing of solid lipid tablets from emulsion gels. Int. J. Pharm. 597, 120304 https://doi.org/10.1016/j.ijpharm.2021.120304.

Korelc, K., Larsen, B.S., Gašperlin, M., Tho, I., 2023. Water-soluble chitosan eases development of mucoadhesive buccal films and wafers for children. Int. J. Pharm. 631, 122544 https://doi.org/10.1016/j.ijpharm.2022.122544.

Kozlovskaya, L., Popilski, H., Gorenbein, P., Stepensky, D., 2015. *In vitro* toxicity of infusion sets depends on their composition, storage time and storage conditions. Int. J. Pharm. 489, 285–293. https://doi.org/10.1016/j.ijpharm.2015.04.065.

Kuraray Poval. URL https://www.kuraray-poval.com/products/kuraray-poval/kuraray-poval-lm (accessed 27.02.2023).

Macedo, R.O., do Nascimento, T.G., Veras, J.W.E., 2001. Comparison of generic hydrochlorothiazide formulations by means of Tg and DSC coupled to a photovisual system. J. Therm. Anal. Calorim. 64, 757–763. https://doi.org/10.1023/A:1011504730402.

Mansur, H.S., Sadahira, C.M., Souza, A.N., Mansur, A.A.P., 2008. FTIR spectroscopy characterization of poly (vinyl alcohol) hydrogel with different hydrolysis degree and chemically crosslinked with glutaraldehyde. Mater. Sci. Eng. C 28, 539–548. https://doi.org/10.1016/j.msec.2007.10.088.

Merekalova, N.D., Bondarenko, G.N., Denisova, Y.I., Krentsel, L.B., Litmanovich, A.D., Kudryavtsev, Y.V., 2017. Effect of chain structure on hydrogen bonding in vinyl acetate – vinyl alcohol copolymers. J. Mol. Struct. 1134, 475–481. https://doi.org/10.1016/j.molstruc.2016.12.094.

Moritani, T., Fujiwara, Y., 1977. 13C-and 1H-NMR investigations of sequence distribution in vinyl alcohol-vinyl acetate copolymers. Macromolecules 10, 532–535.

Ph. Eur. 11.2, 2023. EDQM. Council of Europe, Strasbourg, France.

Pitzanti, G., Mathew, E., Andrews, G.P., Jones, D.S., Lamprou, D.A., 2022. 3D Printing: an appealing technology for the manufacturing of solid oral dosage forms. J. Pharm. Pharmacol. 74, 1427–1449. https://doi.org/10.1093/jpp/rgab136.

Prasad, D.E.V, Chauhan, H., Atef, E., 2014. Amorphous stabilization and dissolution enhancement of amorphous ternary solid dispersions: combination of polymers showing drug – polymer interaction for synergistic effects. J. Pharm. Sci. 103, 3511–3523. https://doi.org/10.1002/jps.24137.

Preis, M., Woertz, C., Kleinebudde, P., Breitkreutz, J., 2013. Oromucosal film preparations: classification and characterization methods. Expert Opin. Drug Deliv. 10, 1303–1317. https://doi.org/10.1517/17425247.2013.804058.

Qureshi, D., Sahoo, A., Mohanty, B., Anis, A., Kulikouskaya, V., Hileuskaya, K., Agabekov, V., Sarkar, P., Ray, S.S., Maji, S., Pal, K., 2021. Fabrication and characterization of poly (Vinyl alcohol) and chitosan oligosaccharide-based blend films. Gels 7, 55. https://doi.org/10.3390/gels7020055.

Rahman, J., Quodbach, J., 2021. Versatility on demand – the case for semi-solid micro-extrusion in pharmaceutics. Adv. Drug Deliv. Rev. 172, 104–126. https://doi.org/10.1016/j.addr.2021.02.013.

Sjöholm, E., Mathiyalagan, R., Lindfors, L., Wang, X., Ojala, S., Sandler, N., 2022. Semi-solid extrusion 3D printing of tailored ChewTs for veterinary use - a focus on spectrophotometric quantification of gabapentin. Eur. J. Pharm. Sci. 174, 106190 https://doi.org/10.1016/j.ejps.2022.106190.

Squillace, O., Fong, R., Shepherd, O., Hind, J., Tellam, J., Steinke, N.J., Thompson, R.L., 2020. Influence of PVAc/PVA hydrolysis on additive surface activity. Polymers 12, 205. https://doi.org/10.3390/polym12010205 (Basel).

Taylor, L.S., Langkilde, F.W., Zografi, G., 2001. Fourier transform Raman spectroscopic study of the interaction of water vapor with amorphous polymers. J. Pharm. Sci. 90, 888–901. https://doi.org/10.1002/jps.1041.

Teixeira, L., de, S., Chagas, T.V., Alonso, A., Gonzalez-alvarez, I., Bermejo, M., Polli, J., Rezende, K.R., 2020. Biomimetic artificial membrane permeability assay over franz cell apparatus using bcs model drugs. Pharmaceutics 12, 988. https://doi.org/10.3390/pharmaceutics12100988.

van der Velden, G., Beulen, J., 1982. 300-MHz 1H NMR and 25-MHz 13C NMR investigations of sequence distributions in vinyl alcohol-vinyl acetate copolymers. Macromolecules 15, 1071–1075. https://doi.org/10.1021/ma00232a022.

WHO Model List of Essential Medicines for Children, 2021. URL https://www.who.int/publications/i/item/WHO-MHP-HPS-EML-2021.03 (accessed: 21.1.2023).

Yadav, A., Chaudhary, R., Singh Bahota, A., Prajapati, P., Pandey, J., Narayan, A., Tandon, P., Vangala, V.R., 2023. Spectroscopic and quantum chemical investigations to explore the effect of intermolecular interactions in a diuretic drug: hydrochlorothiazide. Spectrochim. Acta Part A Mol. Biomol. Spectrosc. 285, 121931 https://doi.org/10.1016/j.saa.2022.121931.